Carbon abundance in the Milky Way Galaxy

Calum MacPherson

Lund Observatory
Lund University

2021-EXA180

Degree project of 15 higher education credits
June 2021

Supervisor: Thomas Bensby

Lund Observatory
Box 43
SE-221 00 Lund
Sweden

Abstract

Carbon is the fourth most abundant element after hydrogen, helium and oxygen. It is a product of stellar nucleosynthesis as well as it being an important bio signature for life; this makes the analysis of carbon very fundamental. The origin of carbon and the relative contributions from massive and low-to-intermediate mass stars in producing it is still under debate. The principal focus of this thesis is to analyse the carbon abundance in the Milky Way. Through the synthetic spectral analysis of five carbon lines of 5052.1 Å, 5380.3 Å, 6587.6 Å, 7111.5 Å, and 7113.2 Å in tandem with high resolution (R = 40 000 - 110 000) and high signal to noise ratio (S/N = 150 - 300) observed spectra, we can determine the carbon abundances of the stars in the sample. In this thesis, the trends of [C/H], [C/Fe], and [C/Mg] versus [Fe/H] as well as, [C/O] versus [O/H] for 502 type F and G dwarf and subgiant stars will have their carbon abundances analysed. By distinguishing between the galactic thin and thick disks we are able to contrast and compare the galactic evolution of carbon. It was found that for [C/H], [C/Fe], and [C/Mg] versus [Fe/H] there was a distinctive overlap in thin and thick disks. For [C/O] versus [O/H] there was a major disparity in the trends of the thin and thick disks. The interpretation of these results leads us to believe the origin of carbon and its contribution is a combination of both low-to-intermediate mass stars and massive stars. Massive stars are believed to contribute more carbon at earlier ages in the universe where as low to intermediate mass stars contribute more in later stages. This interpretation of the results is in line with other recent findings of carbon abundances; typically, it has been found that there is a combination of contributions from massive and low-to-intermediate mass stars but these relative contribtutions are still disputed.

Populärvetenskaplig beskrivning

The question of the origin of carbon in the Milky Way is widely debated and not completely settled. Carbon is the fourth most abundant element after hydrogen, helium and oxygen respectively, yet we still struggle to conclude the main source of carbon in the Milky Way.

It is important to study carbon, since it is a by-product of galactic nucleosynthesis in which carbon is made from the process of nuclear fusion in stars. Finding the origins of the abundance of carbon for stars in the Milky Way will help in understanding the evolution of the universe and will help facilitate further research in the field of astrobiology, since carbon is known as a strong indicator for organic life. The main question up for debate is then whether the main contributor of carbon in the Milky Way is from one of two categories of stars. The first category, known as the low/intermediate mass stars, are thought to contribute carbon by stellar winds stripping the carbon in their atmosphere out in to the interstellar medium. This is much like how a tornado would strip away anything in its path out into the open. These low/intermediate mass stars are relatively cold and live for billions of years, some as long as the universe itself; their atmospheres act as time capsules that can be analysed, as they remain unchanged since their birth. The other category of stars are the high mass stars. These types of stars are a lot hotter; more heat means they run out of fuel a lot faster than colder stars, which in turn means they live in the time scale of millions of years rather than billions. Such hot stars build up an onion-like layer of elements through nucleosynthesis over millions of years of nuclear fusion. This is possible due to extraordinary temperatures well above 100,000,000 K (which is around 17,500 times hotter than the surface of the sun) that cannot be reached by low/intermediate mass stars. Hot stars then contribute carbon by supernovae explosions, the enriched metallic guts of the star are ejected into the interstellar medium when the star reaches the final stages of its life.

Since many different papers indicate a different form of contribution of carbon in the Milky Way, the results of this project hopes to bring us closer to the true origin of carbon in the Milk Way. We do this by generating artificial spectras of different carbon lines using a specialised programming software, one can then find the different carbon abundances of several stars. The results are then plotted in order to visualise different trends.

Contents

List of Figures

List of Tables

Chapter 1

Introduction

Carbon is the fourth most abundant element in the universe after hydrogen, helium and oxygen but its origin is not fully understood. The origin of carbon being contributed from low, medium or high mass stars is still widely debated. It is useful to study since it is a by-product of galactic nucleosynthesis making it important in the study of stellar evolution. All elements undertake different nucleosynthetic pathways, and therefore different processes and timescales can be deduced by analysing elemental abundances.

It has been revealed that the Milky Way has two distinct stellar populations, a thick disk and a thin disk. High-resolution spectroscopic studies indicate that most stars with thick disk kinematics are older than those with thin disk kinematics (e.g. Bensby et al. (2014)). The two population possess different metallicities, ages and kinematics, and it is thus useful to categorise the analysed stars into either group to be able to compare the chemical evolution histories of both disks. The investigation of these disks can be combined with abundance determination and will allow for a more rigorous understanding of the galactic evolution of the Milky Way.

Some papers such as Franchini et al. (2020) found indication that carbon in the Milky Way is produced from both massive and low/intermediate mass stars. Gustafsson et al. (1999) found that carbon is mainly contributed from stellar winds of massive stars. Other papers such as Bensby & Feltzing (2006) contrarily indicate a higher carbon contribution from low mass stars. Over the years many research paper have found different trends, results and regimes regarding the carbon abundance values. Nissen et al. (2014) and Franchini et al. (2020) found that the [C/Fe] versus [Fe/H] had a clear distinction between the thick and thin disks. Bensby & Feltzing (2006) found a flat and merged trend of [C/Fe] versus [Fe/H] for thin and thick disk stars.

Previous papers that attempt to find carbon abundances, base their carbon abundances on different transition line. There are many different carbon lines but a lot of them are molecular lines which are more stable and therefore electron transitions are less likely and there are also few that lines that are reliable. Some transition lines such as the [C I] line at 872.7 nm are prone to Fe I blending and it is generally very weak. Other lines do not suffer from blending but are sensitive to errors. The differing results for carbon abundances is due to an array of reasons. The fact that the spectral lines invoked to spectroscopically

analyse the carbon abundances, e.g. atomic lines (C I) or molecular lines e.g. (C_2, CH) have differing characteristics, depending on star types, sensitivity to 3D and NLTE effects and blending.

In this thesis we use five difference carbon lines of: 5052.1 Å, 5380.3 Å, 6587.6 Å, 7111.5 Å, and 7113.2 Å. Using high resolution spectra, we can study the chemical composition of several main sequence F and G spectral type stars (expected lifetime of 10 Gyr) whose atmospheres remain unchanged since their creation billions of years ago and accentuate conclusions about the different thin and thick disk star populations. The analysis will be compared to chemical evolution models and this will allow us to better grasp the origin of carbon in the Milky Way. In this thesis additional trends based on: [C/H], [O/H] and [O/Fe], versus the metallicity [Fe/H] as well as [C/O] and [Fe/O] versus [O/H], and finally [C/Mg] versus [Mg/H] will be analysed. The majority of literature includes the [C/O] versus [O/H] abundance as oxygen is exclusively produced in massive stars on a relatively short timescale and therefore serves as a way to contrast and compare the trends of carbon and oxygen and what timescale they chemically enrich the Milky Way.

In the next section, the process and methodology of analysing the stellar samples will be described. Section 3 will present the carbon abundance analysis. Section 4 discusses the results of the carbon abundance and section 5 and 6 will discuss the implications of these results and the conclusions we can extrapolate from these results.

Chapter 2

Stellar Sample

The sample of stars analysed in this thesis consist of 502 dwarf and subgiant stars (taken from Bensby et al. (2014)) of the spectral class F and G; this means their lifespans (around 10 Gyr or more) are comparable to the age of the universe itself. We can thus assume that most if not all F and G type stars that have been created still exist. This is useful to us because the atmospheres of these stars remain untouched since their creation giving us insight into the evolution of the chemical composition of the Milky Way in earlier times.

The stars were observed with the high-resolution spectrograph MIKE: Bernstein et al. (2003), giving spectras with resolution, R = 45 000 to 64 000 and a signal-to-noise ratio (S/Ns) of over 200. [1].

2.1 Stellar Parameters and abundances

The stellar parameters, data reduction, stellar ages, stellar masses and abundance analysis of 13 elements (O, Na, Mg, Al, Si, Ca, Ti, Cr, Fe, Ni, Zn, Y, Ba) was previously analysed by Bensby et al. (2014), the reader is directed to this paper for further information regarding the analysis of these parameters. The stellar parameters were deduced predominantly by using equivalent width measurements, by fitting Gaussian profiles to the observed line profiles together with one-dimensional (1D), plane-parallel, local thermodynamical equilibrium (LTE) model stellar atmospheres calculated using the Uppsala MARCS code (Gustafsson et al. (1975); Edvardsson et al. (1993); Asplund et al. (1997)).

The effective temperature T_{eff} is characterised as the surface temperature of a blackbody that has the same luminosity per area as the star. The easiest way to determine the T_{eff} is by excitation balance of abundances from Fe I. The reason we use Fe I lines is because they are the most common spectral line in a stellar spectra, and the lines span over a huge range of wavelengths. In the analysis, non-local thermodynamical equilibrium (NLTE) corrections derived from Lind et al. (2012) were applied to all Fe I abundances.

[1]The Bensby et al. (2014) sample consists of 714 stars measured with many different spectrographs. Due to the constraints of a bachelor thesis the stars only measured by the MIKE spectrograph were used

The surface gravity log g is defined as the acceleration experienced at the surface at the equator. The log g is determined with the stipulation that (in contrast to excitation balance) there is ionisation balance between abundances from Fe I and Fe II lines. This means that the Fe abundance of a stars comes to be the same whether we use Fe I or Fe II lines. We can determine log g combining the luminosity [2] and the definition of the surface gravity [3] and knowing that we have relative relation of the luminosity of a star and the Sun. [4]

The microturbulence (ξ_t) is a mechanism that causes turbulence over a short scale, affecting the line broadening (as well as natural line broadening from Heisenberg's uncertainty principle and pressure broadening). The kinematical motion of gas particles induces a Doppler shift in which depending on the observer increases or decreases the wavelength observed. The ξ_t parameter, is acquired with the prerequisite that abundances from Fe I lines are independent of line strength.

The stellar ages were deduced by utilising a fine grid of α-enhanced Yonsei-Yale (Y2) isochrones by Demarque et al. (2004). By considering the relative errors in the other parameters such as T_{eff} log g, and [Fe/H], an age probability distribution can be calculated for all of the 502 stars.

2.2 Properties of the Stars

2.2.1 Kinematical properties

One way of displaying the kinematical properties of the stars is the use a Toomre diagram which shows the kinematical distribution of our sample. The Toomre diagram for this sample is shown in 2.1. A star is likely to be a thin disk star if its total velocity with respect to the Sun is less than approximately 50 kms^{-1}. Stars with velocity ranging from approximately 70 kms^{-1} to 180 kms^{-1} are likely to be thick disk stars. The total velocity is defined as $v_{\rm tot} \equiv (U^2_{\rm LSR} + V^2_{\rm LSR} + W^2_{\rm LSR})^{1/2}$ where LSR is the local standard of rest in which stars that have a perfectly circular orbit about the galactic centre would have zero velocity in that LSR frame.

[2] Luminosity, $L = 4\pi\sigma T^4 R^2$, where T is the effective temperature and R is the stellar radius.

[3] Surface gravity, $g = GMR^{-2}$, where G is the gravitational constant, M is the stellar mass, and R is the stellar radius.

[4] $log\frac{L_\odot}{L} = 0.4(M_{bol} - M_{bol\,\odot})$

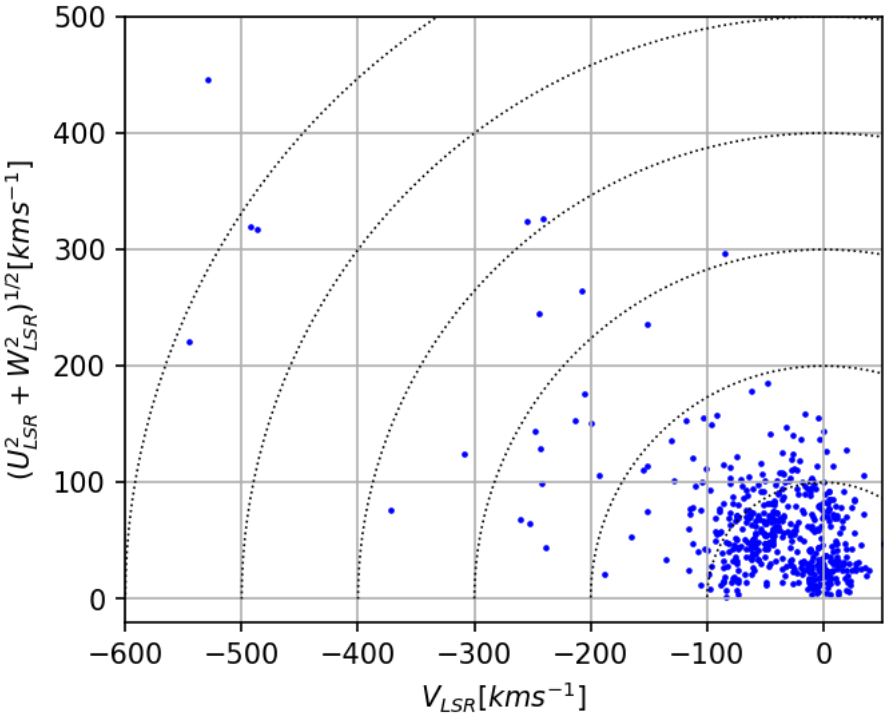

Figure 2.1: Toomre diagrams showing the velocity distribution of the stars used in the carbon abundance analysis

We can use a combination of the kinematical properties to classify the sample into a probability ratio of a star being either a thick disk or thin disk star. The ratio is known as the TD/D where TD represents the thick disk stars and D represents the thin disk stars. The ratio categorises the probabilities of stars being either a thick disk (TD) or thin disk (D) based on certain criteria. Stars with a TD/D greater than 2 are thought to be thick disk stars whereas stars with a TD/D less than 0.5 are thought to be thin disk stars which can be seen in 2.2. The probability ratios presented here are based on the thin and thick disk normalisations and velocity dispersions calculated from Bensby et al. (2014).

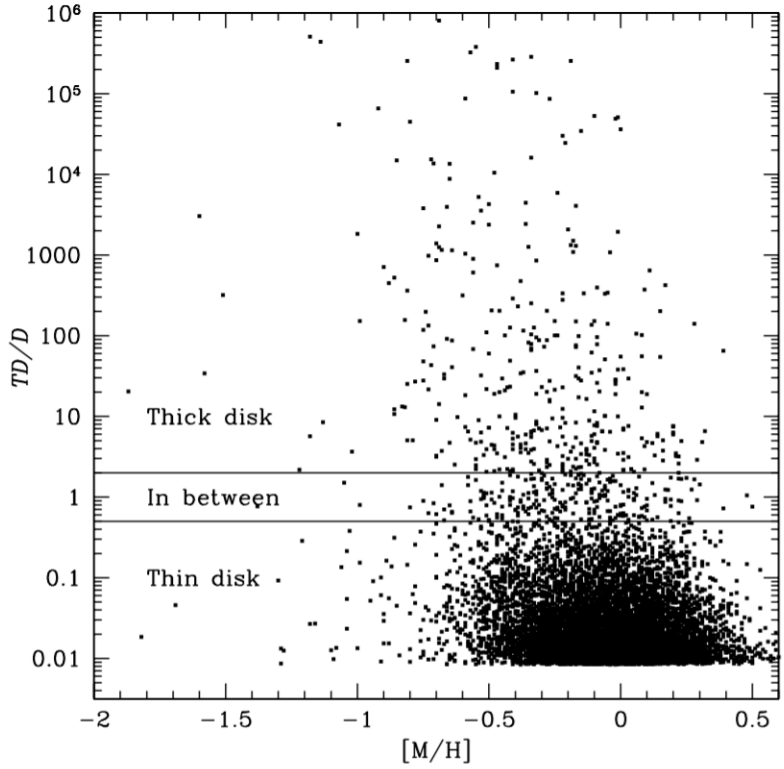

Figure 2.2: This figure is adapted from Bensby et al. (2014) and shows the kinematical thick disk to thin disk probability ratio versus metallicity for the approximately 14 000 stars in the Geneva Copenhagen Survey by Nordström et al. (2004). Here, stars with a TD/D greater than 2 are thought to be thick disk stars whereas stars with a TD/D less than 0.5 are thought to be thin disk stars.

2.2.2 Other Ways of Classifying Thin and Thick Disk Stars

The other approach classifies the stars by age; an age greater than 8 Gyr is classified as a thick disk star and an age below 8 Gyr is classified as a thin disk star. Navarro et al. (2011) argued that it is better to classify stars based upon elemental abundances rather than kinematics. The kinematical approach leads to overlaps of kinematical properties in the thick and thin disk.

It has been suggested by Haywood et al. (2013) that the amount of α enhancement in a star can be used as a proxy for the age of a star. As can be seen in figure 2.3 there is a dividing line that separates the thick and thin disk populations. At high α levels we have the oldest stars, as a result, we have stars that could be associated with the thick disk. There are also remarks regarding the metallicities of thin disk stars below [Fe/H] $\approx$ -0.7 e.g. Reddy et al. (2003). The current literature agrees with this sample as no thin disk stars are below the threshold. Thin disk stars below this value have not truly been found in the current literature, therefore, it can be deduced that [Fe/H] $\approx$ -0.7 serves as a

lower limit for thin disk stars. Overall, the simplest and, perhaps, the most effective way to classify the stars is with age as the data is readily available from Bensby et al. (2014) and thus the other ways of classifying the stars are not used.

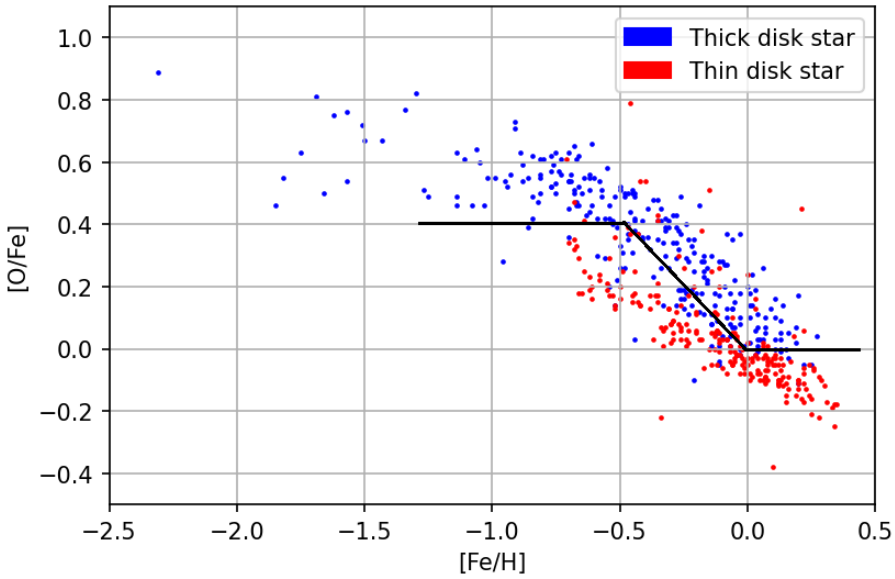

Figure 2.3: Figure showing the [O/Fe] versus [Fe/H] where the stars are classified by age in which the red stars are the stars younger than 8 Gyr and the blue stars are the stars older than 8 Gyr. The data is taken from Bensby et al. (2014).

The criterion to define the stars in this thesis is chosen to be based upon the age. Due to the aforementioned problems of the kinemtatical approach the age criterion makes the most sense to use as it acts as a reliable indicator and is a simple and practical way to classify stars relative to the chemical abundance.

Chapter 3

Carbon Abundance Analysis

3.1 Atomic data and model atmospheres

In this analysis five carbon transition lines were selected, these transition lines are found at 5052.1 Å, 5380.3 Å, 6587.6 Å, 7111.5 Å and 7113.2 Å, (the regions are shown in figure 3.2). The atomic data for all carbon transition lines were acquired from the VALD (Piskunov et al. (1995);Ryabchikova et al. (1997);Kupka et al. (1999);Kupka et al. (2000)) database. The carbon transition data could then be used with a specialised software known as SME Valenti & Piskunov (1996) to be further analysed. SME was made compatible with Python Wehrhahn & Jeff (2021) into a package called PYSME and it is able to calculate synthetic spectra based on the known transition lines from the VALD database, and in tandem with this, the MARCS model stellar atmospheres from Gustafsson et al. (2008) is used to allow us to generate synthetic spectra that will be compared to the observed spectra.

Of the 502 stars 5 of them had absorption lines that were too weak to measure leaving in total 497 stars.

3.2 NLTE Corrections

A common model used in stellar surveys to approximate stellar abundances is with an LTE approximation. An LTE approximation allows for easier calculations at a cost of accuracy of the results; the LTE approximation is strictly a simplification of what occurs in a stellar atmosphere since it assumes the temperature is constant although it is not; this makes the LTE approximation an unrealistic model to use. NLTE corrections bring us closer to the true abundance values by considering the varying temperatures. Amarsi et al. (2020) found that taking into account the departures from LTE reduces the dispersion in the [A/Fe] versus [Fe/H] (where A represents any element) plane by up to 0.2 dex in dwarf stars signifying significant changes in the true abundance values compared to a model that use an LTE approximation.

3.3 Broadening Parameters

Two parameters known as ν_{macro} which is the macroturbulence (this is similar to the microturbulence but in contrast to the microtrubulence it works over larger scales), and $\nu_{rot}sini$ which gives us the velocity component from the observers line of sight of the stellar rotation. These two parameters are convolved to make a radial-tangential (RADTAN) profile. In cooler stars both parameters are approximately similar, and the resulting broadening can be fitted with a Gaussian curve.

3.4 Analysis

To be able to generate synthetic spectra, the python counterpart of SME known as PYSME requires several inputs. By inputting the aforementioned stellar parameters, the NLTE corrections, the MARCS model atmosphere, and atomic data from the VALD database PYSME is able to compute several synthetic spectra that are compared with the observed spectra.

It should be noted that SME was strictly used as a way of generating synthetic spectra, the fitting of the synthetic spectra to the observed spectra was done outside of SME. For PYSME to generate synthetic spectra we firstly choose our carbon line wavelength e.g 5052.1 Å. With all of the stellar parameters defined it is then possible to start generating synthetic spectra. After selecting our wavelength we input a localised range of ± 0.3 around the absorption peak which is indicated by the dotted red lines in the top panel of 3.1. Ten synthetic spectral lines that slightly differ to each other based on the inputs we give are then generated which are indicated by the grey lines in 3.1. By finding the difference between the ten generated synthetic spectra and the observed spectra (indicated by the solid red line in 3.1) we can see which of the synthetic lines most closely match the observed one. Then, the sum of the squared difference between the synthetic and observed spectra is taken which is known as the χ^2 value. The minimisation of the χ^2 value is then taken as the abundance. In order to generate the synthetic spectra we use the code shown in appendix 1 which also shows how the parameters were defined.

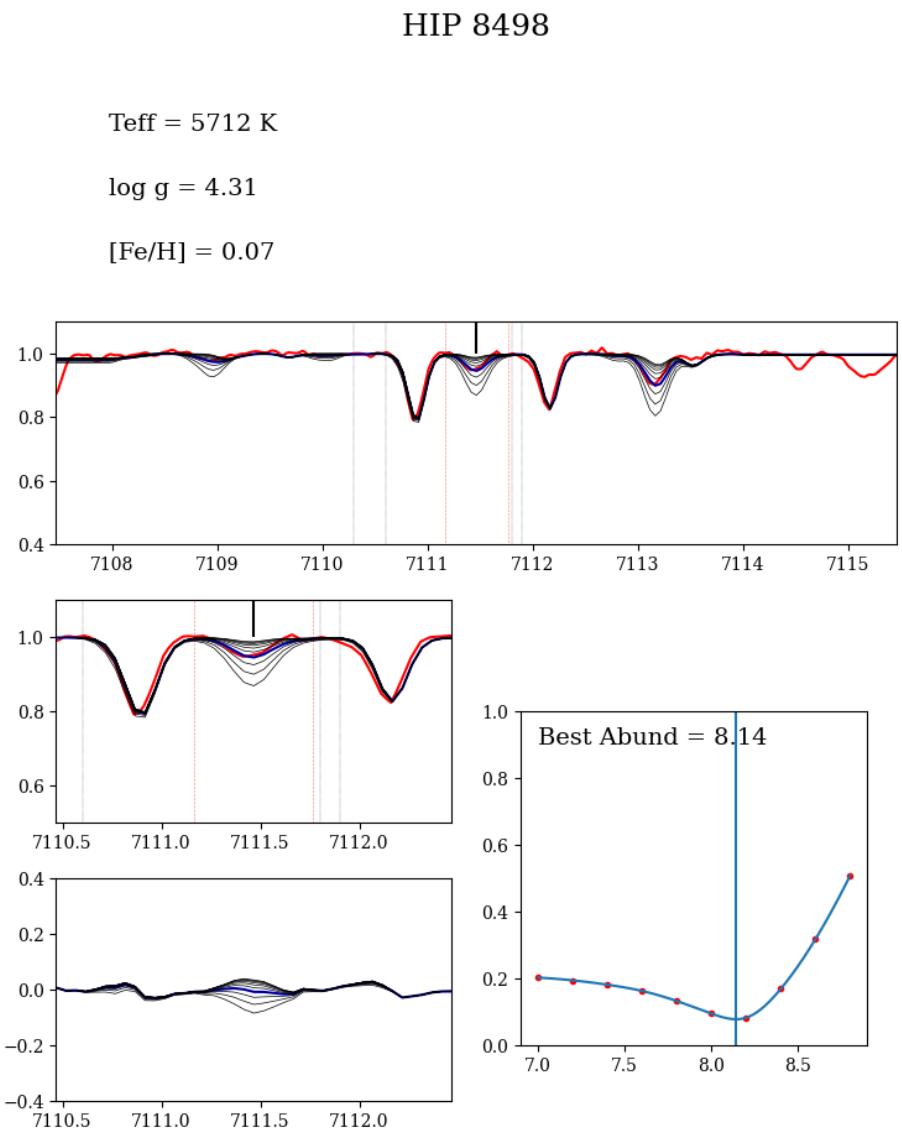

Figure 3.1: A typical fitting from the carbon transition line at 7111.5 Å. The top figure shows the observed spectra in red, the ten generated synthetic spectra; the grey vertical lines show the range in which the continuum was used to normalise the spectra and the red dotted vertical lines show the range from which the absorption speak was measured. The middle left diagram shows an enhanced image localised on the absorption peak. The bottom left figure visualises the differences between the synthetic spectra and observed spectra. The bottom right figure shows the sum of the squared difference between the synthetic and observed spectra this is also known as the χ^2 value. The best abundance is then calculated from the minimisation of the χ^2 value.

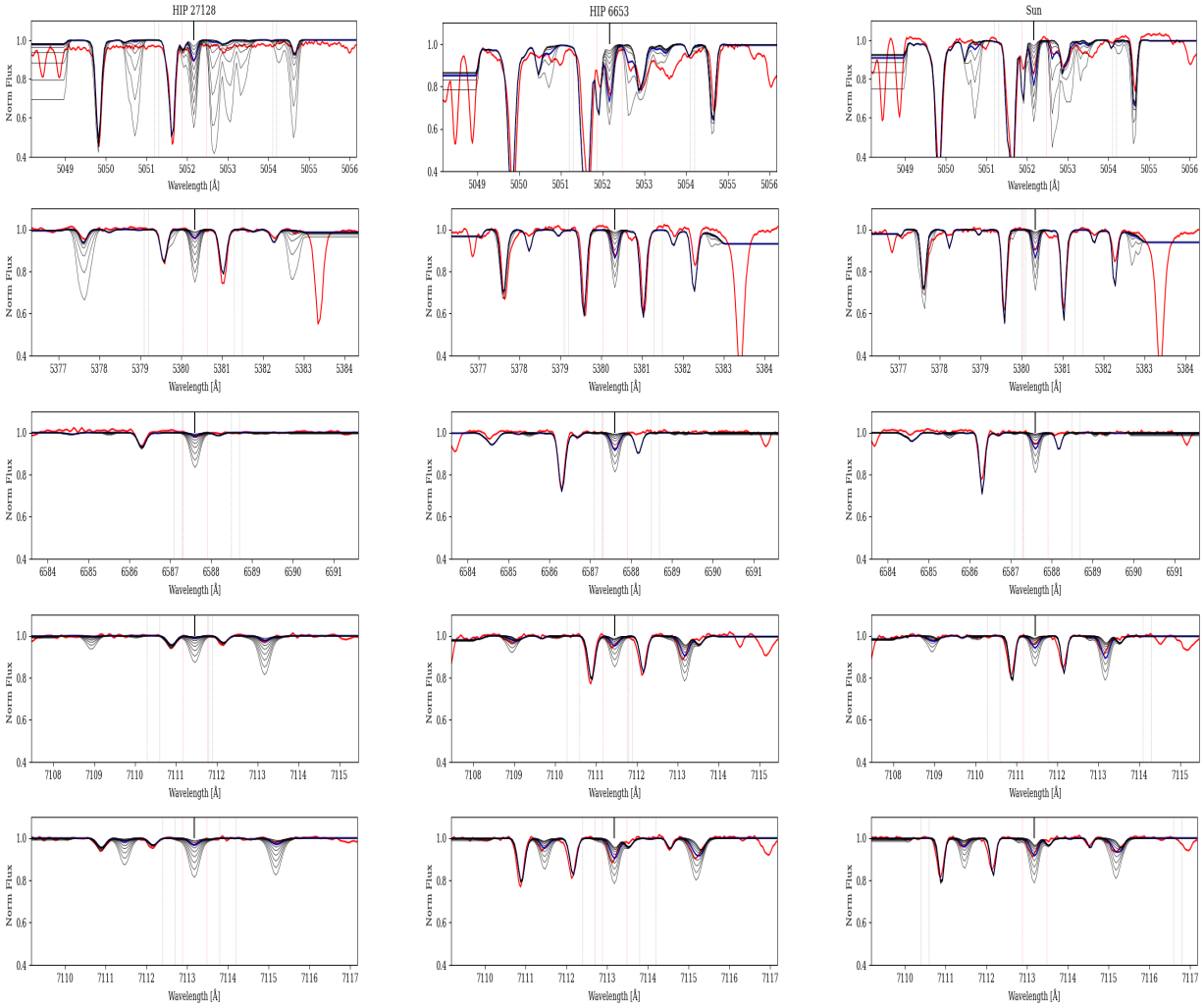

Figure 3.2: Examples of the five different carbon lines used in the abundance analysis. The left column is the carbon lines for a star of low abundance (HIP 27128), the middle column is the carbon lines for a star of high abundance (HIP 6653) and the right column shows the carbon lines for the sun. Each row shows the respective carbon line of 5052.1 Å, 5380.3 Å, 6587.6 Å, 7111.5 Å and 7113.2 Å.

The [C/H] abundance is calculated by finding the abundance of all five carbon transition lines and finding the mean of them [1]. The same is applied for the five carbon transition line found from the sun; the mean abundance found from the sun is then subtracted from the mean abundance found from all of the 497 stars in order to normalise the abundances. The [Fe/H] is taken from Bensby et al. (2014). The [O/H] is calculated by Bensby et al. (2014). The [C/O] versus [O/H] ratio is normally used to compare with carbon in the

[1]Note that the metallicity [Fe/H] is defined as $\log_{10} \frac{N_{Fe}}{N_H}_{star} - \log_{10} \frac{N_{Fe}}{N_H}_{sun}$, where N_{Fe} and N_H are the number of iron and hydrogen atoms per unit volume respectively. By this definition, the Sun will always have a [Fe/H] = 0.

literature since oxygen is exclusively produced in massive stars (Type II supernovae) on a relatively short timescale, the change in [C/O] as a function of [O/H] gives an insight on the production and timescales of carbon since we know the origins of oxygen and it serves as a benchmark of what we expect the trends of carbon to look like. Additionally, we have the [C/Mg] versus [Fe/H] ratio. Mg is an α element amongst other elements (Si, S, Ca and Ti) and can thus serve as a useful element to compare since we have better understandings on the relative contribution and origins of α elements. Different α elements are produced by different stellar processes. For example, all α elements such as Si and Ti are mainly produced from Type II supernovae but also have contributions from Type Ia supernovae.

3.5 Solar Parameters

The analysis of the stars was done relative to the solar parameters. The solar parameters were determined using scattered light reflected from the surface of Jupiter's moon Ganymede. The final calculated carbon abundances are then normalised to the solar carbon abundances using the following $T_{eff} = 5777K$, $\log g = 4.44$ and $\xi_t = 0.88\text{kms}^{-1}$ values. The velocity shift of the sun was calculated manually by shifting the observed spectra to the rest wavelengths.

The solar abundances as previously mentioned were obtained by Bensby et al. (2014) from measuring of the scattered light from Ganymede. Using the same line synthesis techniques as for the main stellar sample, the solar carbon abundance of the sun could be acquired as shown in 3.1.

Table 3.1: A table displaying the calculated carbon abundances of the Sun

Carbon Line Å	5052.2	5380.3	6587.6	7111.5	7113.1
Carbon Abundance	8.21	8.23	8.22	8.21	8.22

Comparing with the literature values from Asplund et al. (2009) they found a $\log \epsilon$ C $= 8.43 \pm 0.05$, whereas in this analysis it was found that the carbon abundance value was $\log \epsilon$ C $= 8.22 \pm 0.04$ This is a difference of approximately 0.2 dex which is quite a significant difference. Since the abundance of the stars are normalised to these solar values the trends, however, still remain the same. The reason for the relatively large difference was unfortunately not discovered, but it is suspected that there was an error made with the programming code (Python) but due to time constraints we were not able to clarify if this was the case.

3.6 Uncertainties

Naturally, these parameters come with a degree of uncertainty that was also calculated by Bensby et al. (2014). The pre-measured parameters: T_{eff}, $\log g$, ξ_t and [Fe/H] are individually modified to take into account uncertainties and is then compared to the first

run where no uncertainties were taken into account by taking the differences. This is done one by one for each parameter and then finally all uncertainties are added up in a quadrature i.e.

$$\sigma_{tot} = \sqrt{\sigma^2_{t_{eff}} + \sigma^2_{logg} + \sigma^2_{[Fe/H]} + \sigma^2_{\xi_t}}.$$

The σ_{tot} is then plotted as a function of each individual parameter. This technique is a simple way to quantify the change in carbon abundances as we change the stellar parameters according to their uncertainties.

When measuring uncertainty, the average measured uncertainty for T_{eff} was $\pm$56; for log g it was $\pm$0.09 dex; for [Fe/H] it was $\pm$0.06 dex; and for the microturbulence it was $\pm$0.1 kms^{-1}. The errors and random errors are mainly as a result of these uncertainties, constituents like the continuum placement on PYSME and the S/N ratio of the stars contribute towards these errors. Other random uncertainties could, for example, be how each individual star reacts differently to a change in a stellar parameter. Systematic errors should be small in this analysis since the analysis was done differentially to the Sun, and thus the errors largely cancel out. The mean of σ_{tot} was found to be $\pm$ 0.04 dex.

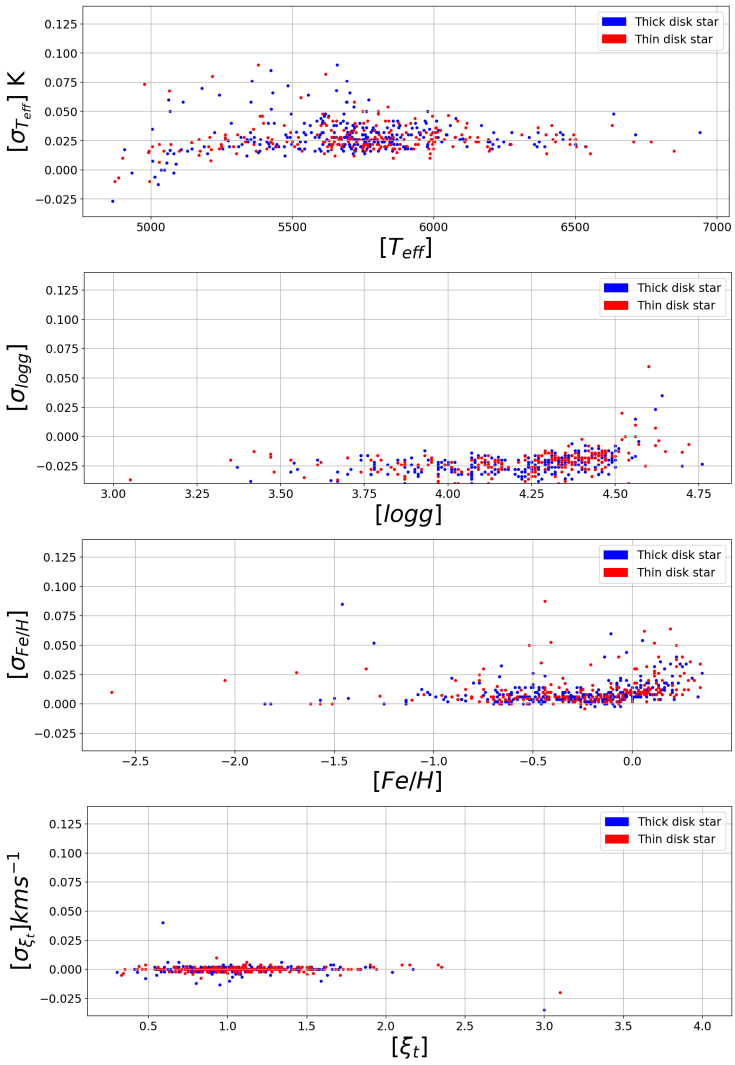

Figure 3.3: The top left figure shows the uncertainty of the T_{eff} as a function of T_{eff}. The top right figure shows the uncertainty of log g as a function of log g. The bottom left figure shows the uncertainty of [Fe/H] as a function of [Fe/H]. The bottom right figure shows the uncertainty of ξ_t as a function of ξ_t.

T_{eff}

The observed trends for the uncertainties of T_{eff} show that the uncertainties increase for lower temperatures, especially around 5500 k and below. Bensby et al. (2014) constrained the stars to only the ones above 5400 K and from this it was found that the bi-modality relation in [α/Fe] was made clearer. At temperatures at approximately 5500 K to 7000 K we see a more constrained distribution of lower uncertainties of mostly $0.025 < \sigma_{tot} < 0.05$. We see fewer stars of higher uncertainty in this range suggesting the stars at these temperature ranges are of higher quality. The high spread of uncertainties across large ranges of

temperatures suggests that the temperature has a relatively high effect on uncertainties.

log g

For the log g uncertainties we have a constant trend where the majority of stars lie within the $0.025 < \sigma_{tot} < 0.05$. At higher log g in the range of $4.25 < log\ g < 4.75$ we see larger uncertainties ranging past $\sigma_{tot} = 0.100$. This would suggest that an increasing log g value leads to higher uncertainties. The log g also has a wide spread of uncertainties across large ranges, although, it is not as prominent as the effects seen in the T_{eff}. This implies that the log g also has a relatively high effect on uncertainties.

[Fe/H]

For the [Fe/H] uncertainties we see a shape akin to a parabola. The uncertainties increase at lower metallicities at around [Fe/H] < -1.0. We also see an increase of uncertainties at [Fe/H] > -0.0. Consistent with the other uncertainties we, again, have a large sample of stars in the band $0.025 < \sigma_{tot} < 0.05$.

ξ_t

Finally, for the ξ_t uncertainties we see a more random distribution where the uncertainties increase. Overall, the spread is small compared to the other parameters suggesting the effects of microturbulence are not felt as much compared to the other parameters. The bulk of the stars lie in the same $0.025 < \sigma_{tot} < 0.05$ band but in a small range of ξ_t ranging mainly from $0.5 < \xi_t < 1.5$. We see that larges uncertainties in this range and a small amount of stars at high uncertainties at $\xi_t > 1.5$.

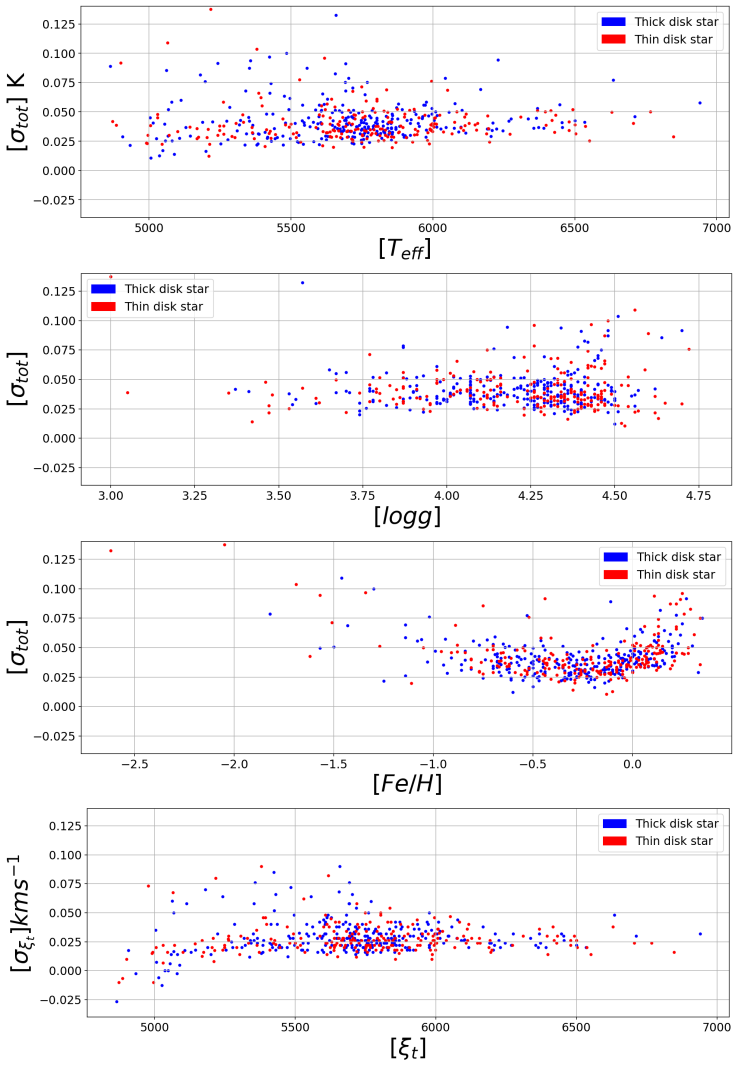

Figure 3.4: The top figure shows the total uncertainty of all four parameters as a function of T_{eff}. The second figure shows the total uncertainty as a function of log g. The third figure shows the total uncertainty as a function of [Fe/H]. Finally, the bottom figure shows the total uncertainty as a function of ξ_t.

Chapter 4

Abundance Results

For each abundance ratio, both a moving average in order to calculate the standard deviation and moving median were calculated in order to contrast and compare the thin and thick disks in a quantitative way. The moving median is less prone to outliers and therefore, it makes sense to use this method in order to extrapolate accurate results. For each elemental abundance comparison, the stars are categorised into both a TD/D and age ratio, where TD/D $>$ 1 is a thick disk star and a TD/D $<$ 1 is a thin disk star. The stars categorised by age are classified as a thin disk star if they are younger than 8 Gyr and a thick disk star if they have an age bigger than 8 Gyr. After some re-evaluation of the results it was chosen only to include the stars classified by the age ratio rather than the TD/D ratio. It should also be noted that it has been found that in previous papers that even small uncertainties on T_{eff} values and magnitudes can result in large age errors, however, due to time constraints we were not able to check what the impact of omitting the lower temperature stars would have had. The standard deviations were added on to the results and display the upper and lower bounds for each segment where the moving mean was calculated. However, in the end it was decided to only use the age classification due to the overlap of kinematical properties found in Bensby et al. (2014).

4.1 [C/H] Versus [Fe/H]

As can be seen from 4.1 it is made evident that the moving median shows that the thin and thick disks have similar carbon values across all metallicities. However, at sub-solar metallicities of approximately [Fe/H] = 0.0 to [Fe/H] = -0.6 in the top right figure we begin to see a minor disparity between the two disks. This is also illustrated when the stars are separated by age. The moving median lines have standard deviations that are on average 0.09 dex. Franchini et al. (2020), in contrast, found that on average, thick-disk stars have larger carbon abundances than thin-disk stars for all values of [Fe/H]. In this thesis it was only found to be true at sub-solar metallicities. The reason behind the difference could possibly be attributed to the fact that the ratio for thick disk compared to thin disk stars measured in their sample is relatively small where only 7.8% of their stars where thick

disk stars. The difference in [C/H] abundance at just below sub-solar metallicities could have implication on the evolution of the thin and thick disks at different metallicities. At sub-solar metallicities, it is observed that there is a wide spread of [C/H] values ranging from [C/H] ≈ -0.9 to [C/H] ≈ 0.0. At super-solar metallicities the spread of [C/Fe] values are narrower falling in the range of [C/Fe] ≈ 0.4 to [C/Fe] ≈ 0.0. It is also observed at super-solar metallicities there is a stronger merge of thin and thick disk stars. At the lowest metallicities we see the biggest spread of [C/H] abundance. This could be possibly attributed due to the fact the resolution for these lower metallicity stars was poor relative to stars of higher metallicity since the carbon lines are too weak to measure in metal-poor stars. The general trend and distribution are in agreement with the findings of Franchini et al. (2020) and Gustafsson et al. (1999).

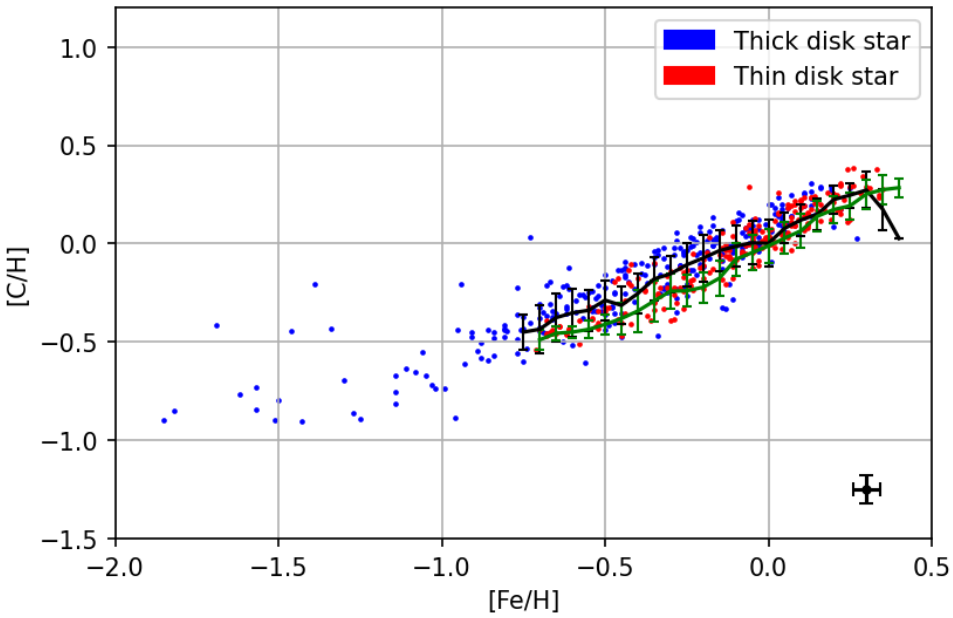

Figure 4.1: The figure shows the relation of [C/H] versus [Fe/H] where each blue point represents a thick disk star and each red point represents a thin disk star. The stars are categorised by age. The black and green lines represent the moving median for thick and thin disk stars respectively. The black error bar in the bottom right corner indicates the calculated average uncertainty for a given star.

In figure 4.2 which shows the [O/H] versus [Fe/H] we see a similar trend but a clearer distinction between the thick and thin disk stars across all metallicities. At super-solar metallicities the disparity between the thin and thick disk stars is smaller than that at sub-solar metallicities

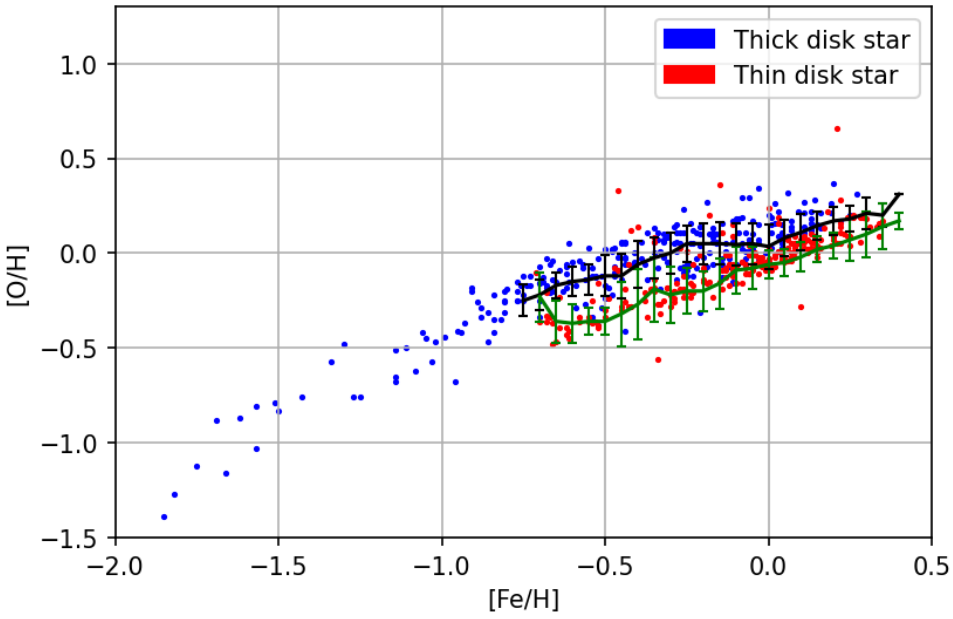

Figure 4.2: The figure shows the relation of [O/H] versus [Fe/H] where each blue point represents a thick disk star and each red point represents a thin disk star. The stars are categorised by age. The black and green lines represent the moving median for thick and thin disk stars respectively.

When observing the individual carbon transition lines in 4.3 we see varying regimes. For the first two carbon lines (5052.2 Å and 5380.3 Å) as well as the fifth (7113.2 Å) we see a pattern that closely resembles the regime we observe in 4.1. For the fourth carbon line, we see a much larger spread of data points especially at [C/H] $<$ -0.5 values. The reason for this is likely due to the weak nature of this line making the results less reliable. For a better average [C/H] versus [Fe/H] relation the values for the fourth line should be omitted and an average [C/H] should be calculated from the first, second, third and fifth lines only.

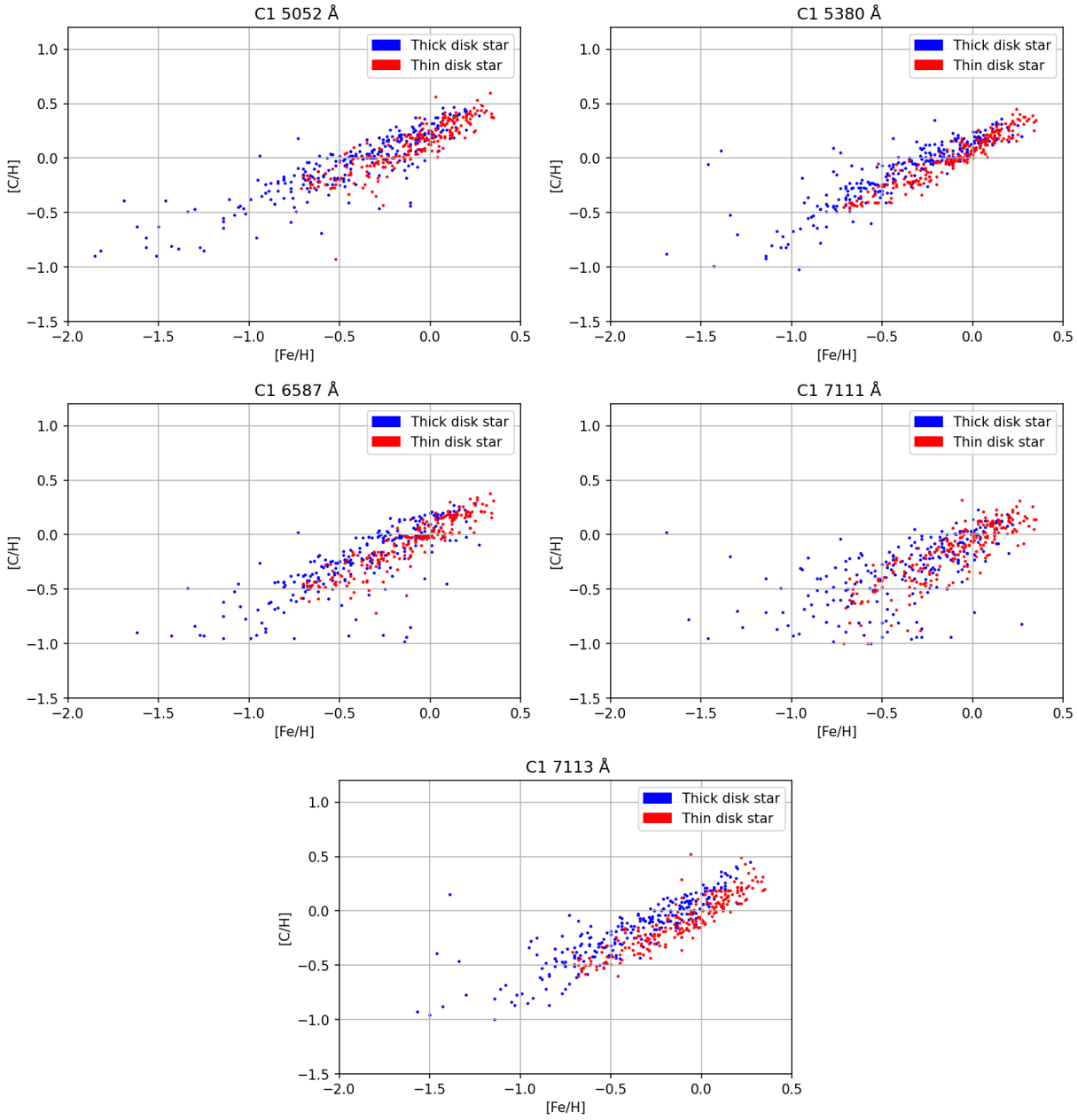

Figure 4.3: The five figures show the five different carbon transition line abundances as a function of metallicity.

4.2 [C/Fe] and [O/Fe] Versus [Fe/H]

Following from the literature an element such as Mg and Ti takes a shape shown in 5.1. Looking at 4.4 we see a vaguely similar pattern shown by the moving median. Carbon is not an α element but the trend shown makes it seem like it behaves closely to an α

element. If we observe the trends shown in 4.4 we see that the thin and thick disks are (similar to the [C/H] versus metallicity) not merged at sub solar metallicites which is not in agreement with the findings of Bensby & Feltzing (2006). The area localised around [Fe/H] ≈ 0.0 to [Fe/H] ≈ -0.5, shows the most disparity between the thick and thin disk. Since this was also observed in the previous abundance ratio it further strengthens the argument that there may be a difference in the chemical evolution of the thick and thin disks at sub-solar metallicities.

In contrast to Bensby & Feltzing (2006) who found that [C/Fe] does not increase with decreasing [Fe/H], it was found that the [C/Fe] increases for decreasing [Fe/H]. The reason for this difference is hard to decisively conclude, however, it is likely due to a very small sample size in Bensby & Feltzing (2006) and they used the the forbidden [C I] line at 872.7 nm. Chiappini et al. (2003) found an almost completely flat trend for [C/Fe] versus [Fe/H]. Again it is difficult to reason why we see this difference as not much detail is given in the analysis with Chiappini et al. (2003) but there differences in the way the stars are modeled which could lead to the differences we see here. Akin to these results, the results found by Gustafsson et al. (1999) also shows that the [C/Fe] increases for decreasing [Fe/H] . Reddy et al. (2006) found that the abundance ratios [C/Fe] for their thick-disk sample stars with [Fe/H] < 0.4 were, on average, larger than for their thin-disk stars of the same [Fe/H]. This is what we also observe here with the top figure in figure 4.4. Nissen et al. (2014) found that their thin-disk stars fall below the thick-disk ones in the [C/Fe] versus [Fe/H] diagram for [Fe/H] ≈ 0.3 and suggested that the two populations merge at higher metallicities which is what was found here. Franchini et al. (2020) found that the thick-disk stars show a higher [C/Fe] than the thin-disk stars for $0.5 <$ [Fe/H] < 0.1, it should also be noted that they obtained a [C/Fe] versus [Fe/H] trend that recalls the behaviour of an α-element versus [Fe/H] but with a less pronounced separation. At super-solar metallicities, the abundance flattens, beginning at approximately solar metallicities. At very low metallicities we again see a big distribution of stars which is again perhaps related to the poor quality of metal-poor stars. The bottom panel of 4.4 shows the [C/Fe] versus [Fe/H] with the weaker fourth carbon line being omitted. The changes are only slight as the only main difference we can see is a slightly tighter relationship with less spread at super-solar metallicities.

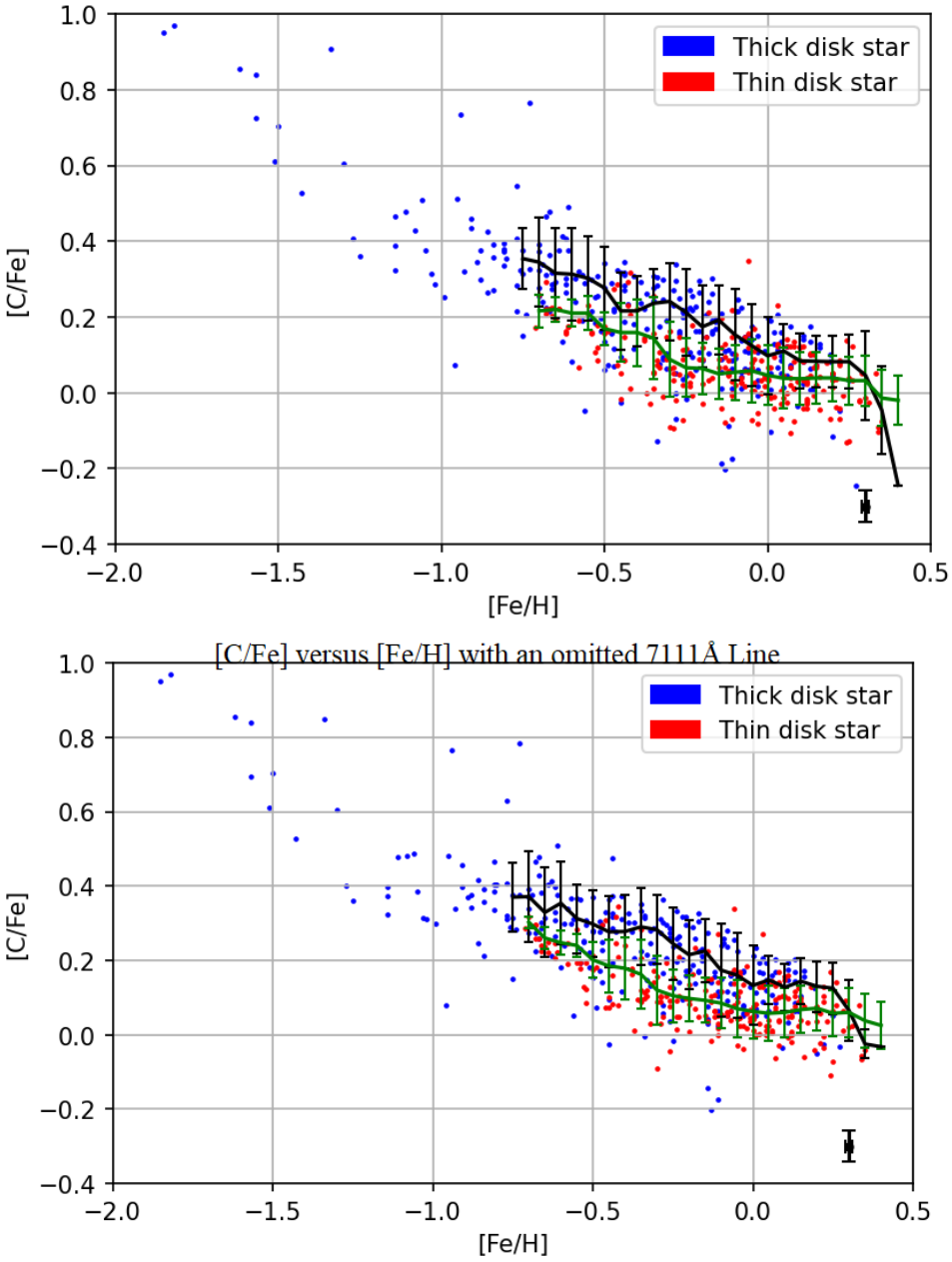

Figure 4.4: The top figure shows the relation of [C/Fe] versus [Fe/H] where each blue point represents a thick disk star and each red point represents a thin disk star. The stars are categorised by age. The black and green lines represent the moving median for thick and thin disk stars respectively. The bottom figure shows all of the same details but the fourth (7111 Å) carbon line has been omitted from the calculation of [C/Fe]. The black error bar in the bottom right corner indicates the calculated average uncertainty for a given star.

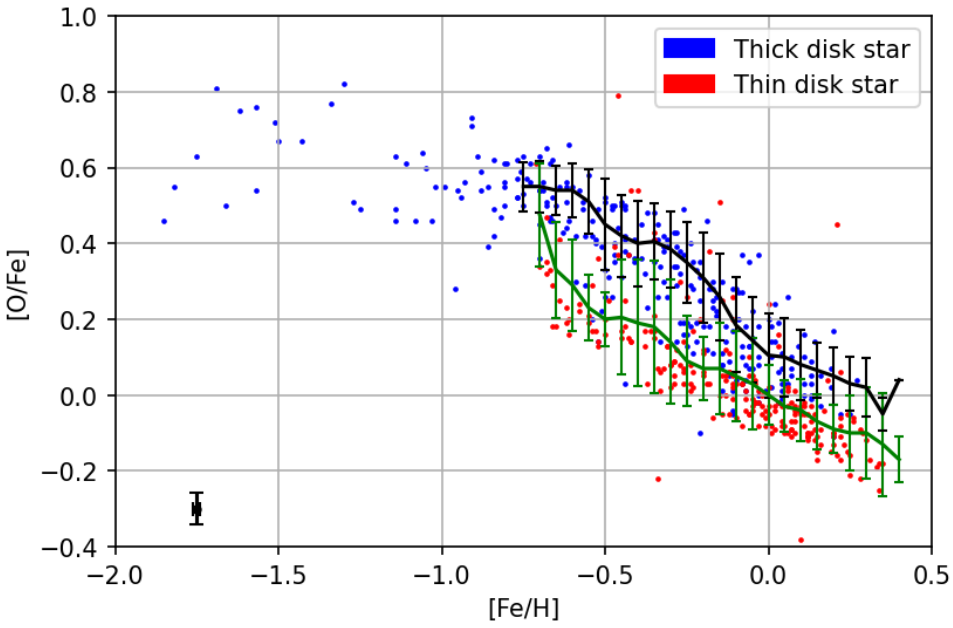

Figure 4.5: This figure shows the relation of [O/Fe] versus [Fe/H] where each blue point represents a thick disk star and each red point represents a thin disk star. The stars are categorised by age. The black and green lines represent the moving median for thick and thin disk stars respectively. The black error bar in the bottom left corner indicates the calculated average uncertainty for a given star. The results for [O/Fe] versus [Fe/H] are taken from Bensby et al. (2014)

4.3 [C/Mg] Versus [Mg/H]

Here we see a very strict overlap with of thin and thick disk regimes. Through the entire metallicity range of -0.6 < [Mg/H] < 0.3 there is a near perfect overlap. At lower metallicities of around -0.9 < [Mg/H] < -0.7 we begin to see the moving median for thick disk stars become more sporadic which is observed in both the TD/D and age classification but is less pronounced in the age classification. Similar to the other trends we see a wide spread of stars at a low [Mg/H] which is again likely due to the aforementioned reasons. Franchini et al. (2020) also found a horizontal distribution but they found a clear separation of the thin and thick disk which is not observed here.

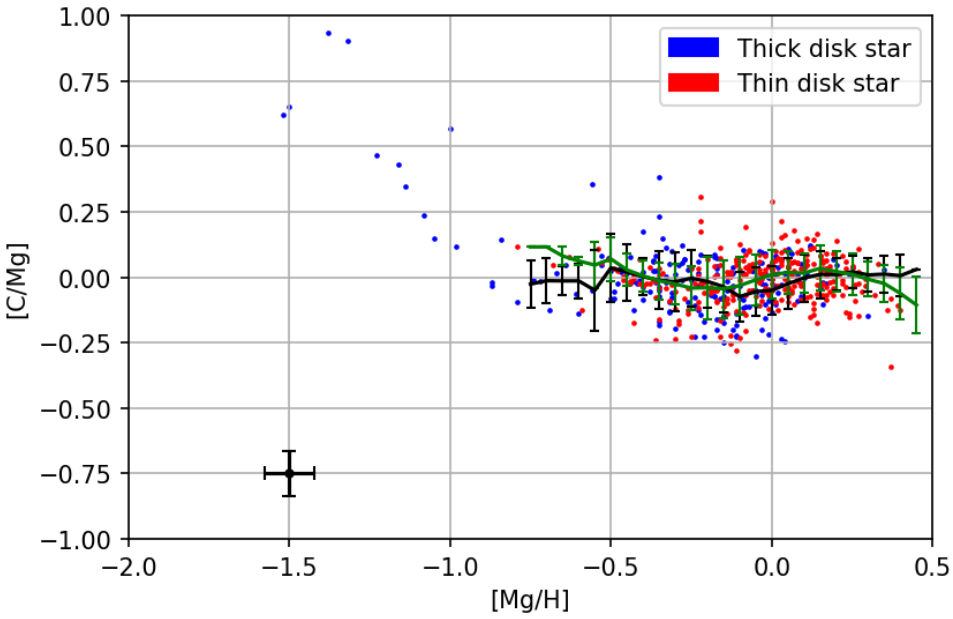

Figure 4.6: This figure shows the relation of [C/Mg] versus [Mg/H] where each blue point represents a thick disk star and each red point represents a thin disk star. The stars are categorised by age. The black and green lines represent the moving median for thick and thin disk stars respectively. The black error bar in the bottom left corner indicates the calculated average uncertainty for a given star.

4.4 [C/O] and [Fe/O] Versus [O/H]

It is clear from the trends observed in 5.2 that there is a relatively large disparity between the thin and thick disk stars in the TD/D ratio classification. Both disks show flat trends across the entire range of metallicities. Comparing these results to Bensby & Feltzing (2006), they also found a separated thin and thick disk regime. However, in contrast to what was found in this thesis, they found that the thin disk shows a shallow increase in [C/O] with [O/H] whilst the thick disc first has a flat [C/O] trend that increases sharply at [O/H] = 0. These trends are not observed here. If we observe the sample classified by age, we see that there is a similar trend as shown in the thick and thin disk classification. This could reveal critical information regarding the chemical evolution models of the thin and thick disks. Beginning at solar metallicities the overall trend of the thick disk is a shallow increase in [C/O] abundance with the age classification. The thin disk has an extremely shallow increase also beginning at solar metallicities. At sub-solar metallicities we see that for decreasing [O/H] we generally do not see a decreasing [C/O].

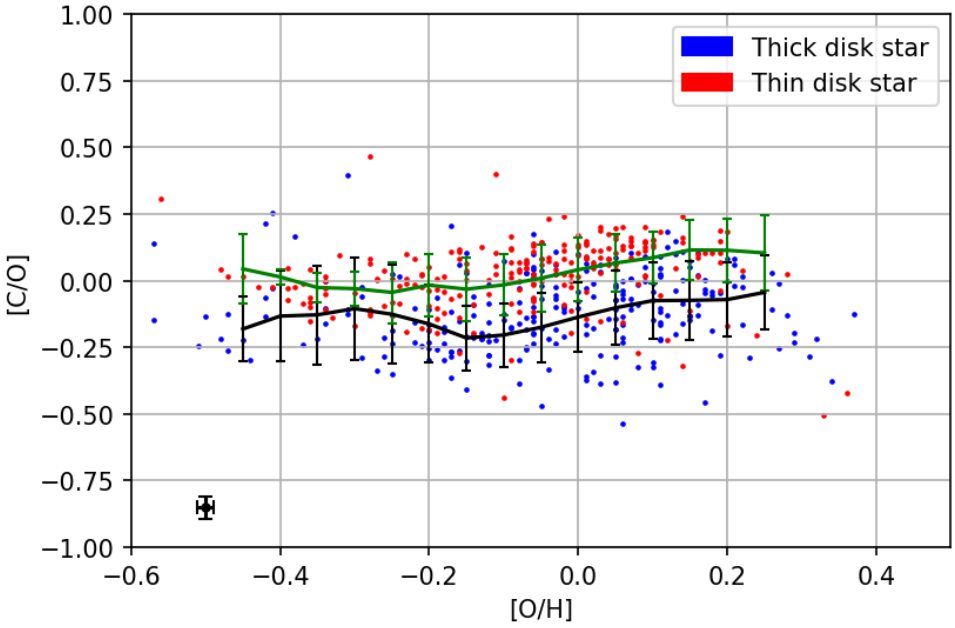

Figure 4.7: This figure shows the relation of [C/O] versus [O/H] where each blue point represents a thick disk star and each red point represents a thin disk star. The stars are categorised by age. The black and green lines represent the moving median for thick and thin disk stars respectively.

Chapter 5

Discussion

Prior to discussing the implications of the observed trends, we shall briefly discuss what the current literature says about carbon. Currently, it is still largely debated what the origin of carbon in the Milky Way is. The main sites of contention are supernovae, novae, Wolf–Rayet stars (Massive stars), low- and intermediate-mass stars in the planetary nebula phase or by super-winds at the end or the red-giant phase. For low mass stars it is thought that their envelopes are blown off by stellar winds prior to becoming white dwarfs. For massive stars it is thought they contribute both by exploding as supernovas and enrich the interstellar medium (ISM) with their interiors i.e. type II supernovas (SN II), and by contributing carbon in their earlier phases, due to their massive radiation-driven winds.

Abundance ratios can serve as an indicator for the aforementioned IMF and SFR parameters, so by comparing carbon with iron which is produced by both type Ia supernova (SN Ia) which results from the mass accretion by a C-O white dwarf and SN II which results from exploding massive stars, we can analyse the chemically evolving thin and thick disk. Oxygen is also an α element which, of course, is also a product of the CNO cycle. It is believed to strictly only be produced in SN II meaning it serves as a useful element to make comparisons with carbon trends.

If the SFR is high, stellar gas will reach a higher [Fe/H] before the first SN Ia occurs, and the position of the downturn at [Fe/H] $>$ -0.5 in the [α/Fe] versus [Fe/H] diagram 5.1 will be at a higher [Fe/H]. The downturn serves as an indication of the SN Ia. The horizontal line where [Fe/H] $<$ -0.5 indicates a time period where α elements were dispersed into the ISM through the explosions of SN II. In this time frame there is an overabundance of α elements being produced relative to iron implying that we have a positive [α/Fe] ratio which we observe in 4.1. If the IMF is favoured towards more massive stars i.e. more contribution from SN II the [α/Fe] would be even higher in the plot and vice versa. Due to the nature of massive stars, they have shorter life spans and SN II will remain the main source of contribution until, given enough time, the SN Ia will start to enrich the ISM. This is observed when the [α/Fe] begins to decline as SN Ia begin to enrich the ISM with higher levels of iron.

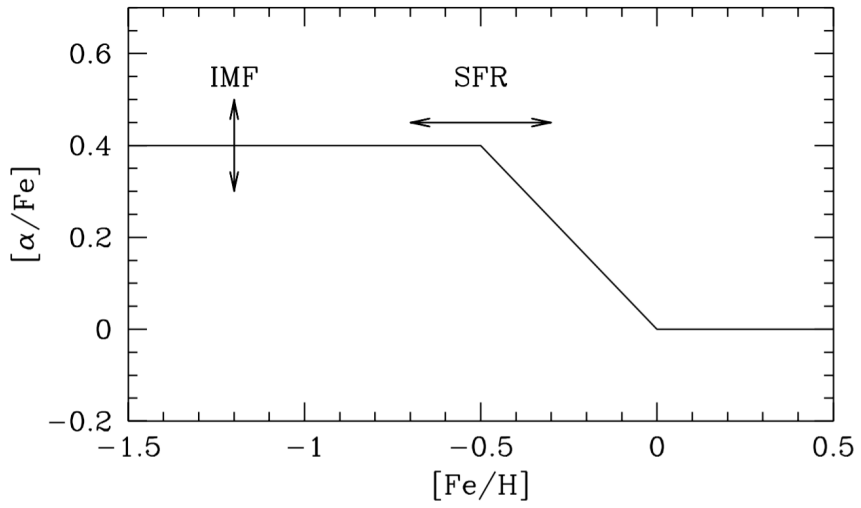

Figure 5.1: A figure displaying how the [α/Fe] ratio is affected by the IMF and SFR.

5.1 Potential source of carbon

Carbon is not a true α element but Reddy et al. (2006) suggested that carbon does in-fact behave like Mg and other α elements, this is reflected in 4.4 where we see a very tight overlap and a horizontal linear relation. Furthermore, the [C/Fe] versus [Fe/H] diagram loosely fits the shape shown in 5.1. Chiappini et al. (2003) suggested that a flat [C/Fe] versus [Fe/H] trend from [Fe/H] $\approx$ -2.2 to solar implied that the main source of carbon is from low to intermediate mass stars. This flat trend is not observed with these results, instead we see an increasing abundance of [C/Fe] for decreasing [Fe/H] and we therefore cannot conclude that the main source of carbon is from low to intermediate stars according to this data set. The thick disk for the [O/Fe] trend shows an over-abundance of oxygen at low metallicities which then subsequently goes into a downturn at [Fe/H] ≈ -0.5. The implications of this are the onset of SN Ia, since oxygen is only produced by SN II the eventual increased Fe production by SN Ia results in a decreasing metallicity as the overabundance of oxygen decreases. The over-abundance pattern observed in [C/Fe] versus [Fe/H] is not observed as we do not see a defining "knee" where we have a downturn of abundance. However, if the [C/Fe] versus [Fe/H] abundance ratio were to be flat, it could be inferred that from the carbon abundances in the thick disk sample that enrichment from carbon happens on the same time-scale as the enrichment from SN Ia. Since we do not have a flat trend, but a trend that more closely resembles [O/Fe] without the over abundance at low metallicities it could be inferred that there are some similarities in the time scale of carbon production with oxygen, to add to this, it could also be speculated that the enrichment of carbon is slightly deviated away from the time scale from the enrichment from SN Ia and isn't as closely associated as previously thought. Gustafsson et al. (1999) stated that if carbon were to be produced solely by SN II then we would expect to see the carbon and oxygen

trends to be the same but we can see that there is a difference in which carbon lacks the over-abundance at low metallicities. But both the distribution and gradient for both thin and thick disk are similar. We can then speculate that it is unlikely from the results that carbon is solely produced by SN II but potentially has some similarities with oxygen owing to the similar looking trends.

Supernovae of Type Ia, which is believed to produce most of the iron, does not contribute significant amounts of carbon e.g. from Nomoto et al. (1997), and the fact that the contributions from SN II are likely not the main source of contributions it should be noted that supernovae are likely not the major source of carbon. Novae should also potentially be ruled out as a major source of the origins of carbon due to the frequency of them occurring and as Gehrz et al. (1998) suggested the mass loss would be too low the enrich the ISM.

If low and intermediate mass stars are important, Chiappini et al. (2003) predicted that there first would be a flat [C/O] plateau for the thick disk that then at roughly solar [O/H] it should sharply increase, to be followed by a shallow thin disk [C/O] trend at higher [C/O] ratios. In these results we do see a flat plateau for the thick disk but there is only a shallow increase following the solar metallicity. The implications of this could suggest that low and intermediate mass stars are not as important as previously thought and more of the carbon could have been contributed from massive stars than anticipated. Comparing the [C/O] versus [O/H] to the [O/Fe] versus [O/H] we see a resemblance in the shape trends, however, we see a much steeper upturn in the [Fe/O] versus [O/H] graph. The resemblance between [C/O] and [Fe/O] in 5.2 could then suggest that carbon and iron originate from objects on similar time scales i.e. from low and intermediate mass stars but since in figure 5.2 we see the sharper upturn we cannot decisively say that carbon and originate on the same time scale. The similarity also strengthens the importance of low and intermediate mass stars as contributors to the carbon enrichment at higher metallicities.

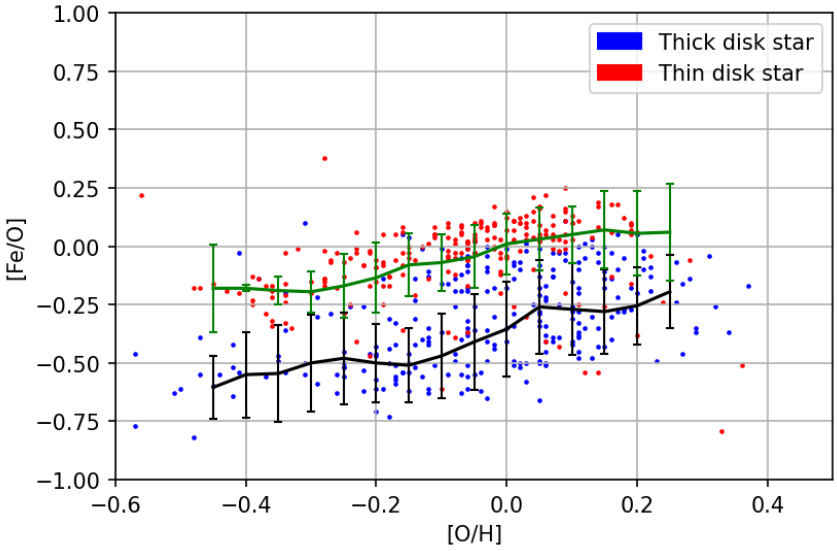

Figure 5.2: This figure shows the relation of [Fe/O] versus [O/H] where each blue point represents a thick disk star and each red point represents a thin disk star. The stars are categorised by age. The black and green lines represent the moving median for thick and thin disk stars respectively. The results for [Fe/O] versus [Fe/H] are from Bensby et al. (2014)

Gustafsson et al. (1999) suggested that an increasing [C/O] versus [Fe/H] as shown in 5.3 is indicative of both massive stars and low to intermediate mass stars contributing carbon. The gradual increase of C/O in the disk, reflects the difference in time-scale between the carbon producing stars and the massive stars producing oxygen.

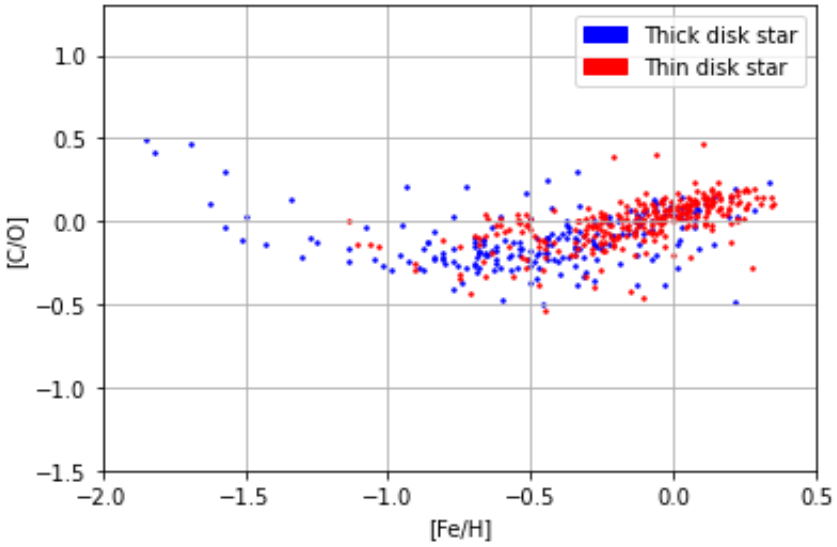

Figure 5.3: A figure displaying the [C/O] versus metallicity abundance ratio where the red and blue points represent the thin and thick disk respectively.

For [C/H] versus metallicity, the assumption that the origin of carbon is from massive stars implies that we get a strong correlation of the carbon abundance with metallicity e.g. Gustafsson et al. (1999). If the age is the dominating factor, determining the carbon abundance in the low to intermediate mass stars case, one would expect a stronger correlation between [C/H] and age. Observing the figure in 4.1 we see a strong correlation between [C/H] and metallicity. A much greater scatter is found in the [C/H] vs. stellar age relation shown in 5.4, this could imply that carbon is much more closely related to the metallicity than age. From this same figure we can also clearly see a distinction in the ages of the thin and thick disk stars, and following from the literature e.g.Spitoni et al. (2019) stated that there is a time frame of 4.3 Gyr between the first and second accretion episodes in where the disks were formed. The oldest thick disk stars have lower [C/H] than the thin disk stars. The trend suggests that carbon is produced at the beginning by massive stars and in more recent times by low mass stars or by high metallicity massive stars attributed by their mass loss in agreement with the findings of Franchini et al. (2020). For [O/H] versus [Fe/H] we see a more shallow trend of oxygen at higher metallicities compared to the [C/H] versus [Fe/H]. The shallower trend indicated a point in time when the contributions from SN II begin to decrease and contributions from iron begins to increase. Since we don't see the same level off with carbon, this suggests that there has to be contributions other than SN II coming from carbon.

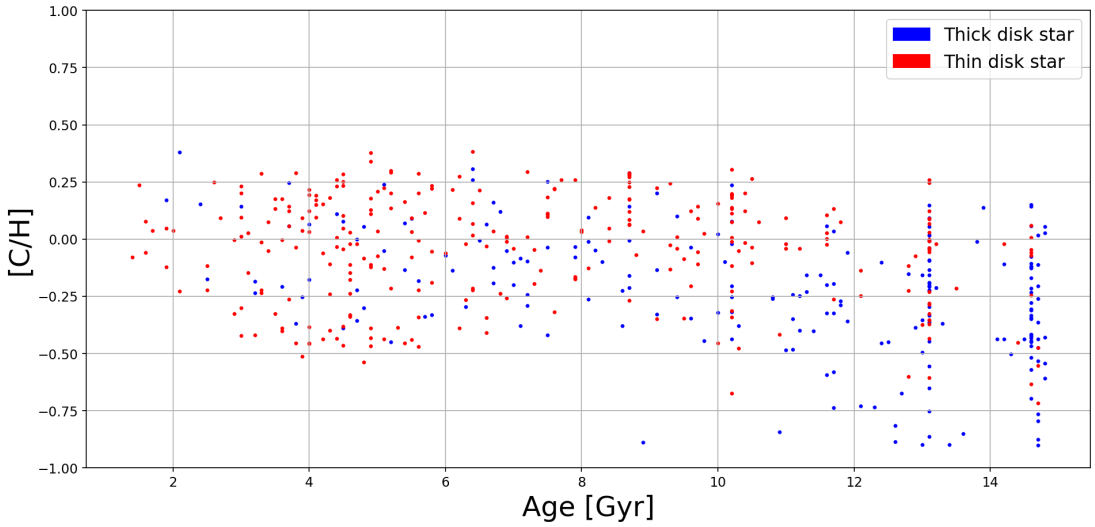

Figure 5.4: A figure showing [C/H] versus age where the red and blue points are the thin and thick disk respectively. The points are classified with the TD/D ratio.

Chapter 6

Conclusion

To summarise, high resolution spectra of 502 F and G type stars had their abundances measured and plotted using five different carbon transition lines which were : 5052.2 Å, 5380.3 Å, 6587.6 Å, 7111.5 Å and 7113.1. After the analysis of the different trends and regimes that the results showed, we came to the following conclusions:

1. The [C/H], [C/Fe] and [C/Mg] versus [Fe/H] all showed a small disparity between the thin and thick disk whereas [C/O] versus [O/H] ratio showed a significant discrepancy.

2. The absence of a flat [C/Fe] versus [Fe/H] trend implied that massive stars may have a more influential role than previously thought and we cannot decisively say that carbon comes exclusively from low and intermediate-mass stars. The similarities between the trends of both the thin and thick disk stars with [O/Fe] versus [Fe/H] implies there could be some similarities between oxygen and carbon production.

3. The positive trend in [C/O] versus [O/H] with the upturn at [Fe/H] ≈ -1.0 suggests that low and intermediate mass stars are important for the enrichment of carbon, however, we see only a shallow increase which could indicate less importance at low and intermediate mass stars.

4. The similarities between [C/O] versus [O/H] to the [O/Fe] versus [O/H] suggests that carbon and iron originate from objects of similar time scales i.e. from low and intermediate mass stars/SN Ia.

5. Following from 5.4 and the current literature, there is a clear distinction in the age of the thin and thick disk.

   To conclude, I still do not think that the origin of Carbon is fully settled but we are getting closer to a final answer. A lot of trends are show large similarities to other papers, yet other trends show minor differences that cannot be fully explained. Some things that could have been done that were not done were to firstly: omit the fourth (7111 Å) carbon line from the calculations; secondly, include the full stellar sample from Bensby et al. (2014); and thirdly, further minimise errors that were generated

by the manual nature of some of the analysis such as the continuum placements and the localised wavelength selection at the absorption peaks. The picture of where carbon comes from is clearer but more research still needs to be done.

Bibliography

Amarsi, A. M., Lind, K., Osorio, Y., et al. 2020, A&A, 642, A62

Asplund, M., Grevesse, N., Sauval, A. J., & Scott, P. 2009, ARA&A, 47, 481

Asplund, M., Gustafsson, B., Kiselman, D., & Eriksson, K. 1997, A&A, 318, 521

Bensby, T. & Feltzing, S. 2006, MNRAS, 367, 1181

Bensby, T., Feltzing, S., & Oey, M. S. 2014, A&A, 562, A71

Bernstein, R., Shectman, S. A., Gunnels, S. M., Mochnacki, S., & Athey, A. E. 2003, in Society of Photo-Optical Instrumentation Engineers (SPIE) Conference Series, Vol. 4841, Instrument Design and Performance for Optical/Infrared Ground-based Telescopes, ed. M. Iye & A. F. M. Moorwood, 1694–1704

Chiappini, C., Matteucci, F., & Meynet, G. 2003, A&A, 410, 257

Demarque, P., Woo, J.-H., Kim, Y.-C., & Yi, S. K. 2004, , 155, 667

Edvardsson, B., Andersen, J., Gustafsson, B., et al. 1993, A&A, 500, 391

Franchini, M., Morossi, C., Di Marcantonio, P., et al. 2020, ApJ, 888, 55

Gehrz, R. D., Truran, J. W., Williams, R. E., & Starrfield, S. 1998, , 110, 3

Gustafsson, B., Bell, R. A., Eriksson, K., & Nordlund, A. 1975, A&A, 500, 67

Gustafsson, B., Edvardsson, B., Eriksson, K., et al. 2008, A&A, 486, 951

Gustafsson, B., Karlsson, T., Olsson, E., Edvardsson, B., & Ryde, N. 1999, A&A, 342, 426

Haywood, M., Di Matteo, P., Lehnert, M. D., Katz, D., & Gómez, A. 2013, A&A, 560, A109

Kupka, F., Piskunov, N., Ryabchikova, T. A., Stempels, H. C., & Weiss, W. W. 1999, , 138, 119

Kupka, F. G., Ryabchikova, T. A., Piskunov, N. E., Stempels, H. C., & Weiss, W. W. 2000, Baltic Astronomy, 9, 590

Lind, K., Bergemann, M., & Asplund, M. 2012, MNRAS, 427, 50

Navarro, J. F., Abadi, M. G., Venn, K. A., Freeman, K. C., & Anguiano, B. 2011, MNRAS, 412, 1203

Nissen, P. E., Chen, Y. Q., Carigi, L., Schuster, W. J., & Zhao, G. 2014, A&A, 568, A25

Nomoto, K., Iwamoto, K., Nakasato, N., et al. 1997, , 621, 467

Nordström, B., Mayor, M., Andersen, J., et al. 2004, A&A, 418, 989

Piskunov, N. E., Kupka, F., Ryabchikova, T. A., Weiss, W. W., & Jeffery, C. S. 1995, , 112, 525

Reddy, B. E., Lambert, D. L., & Allende Prieto, C. 2006, MNRAS, 367, 1329

Reddy, B. E., Tomkin, J., Lambert, D. L., & Allende Prieto, C. 2003, MNRAS, 340, 304

Ryabchikova, T. A., Piskunov, N. E., Kupka, F., & Weiss, W. W. 1997, Baltic Astronomy, 6, 244

Spitoni, E., Silva Aguirre, V., Matteucci, F., Calura, F., & Grisoni, V. 2019, A&A, 623, A60

Valenti, J. A. & Piskunov, N. 1996, , 118, 595

Wehrhahn, A. & Jeff, V. 2021, http://doi.org/10.5281/zenodo.4897051

Appendix A

PYSME Code

```
def hippy(hip, ls):

params = Table.read('table_c3.csv',format='ascii.no_header')
teff = np.float(params[params['col1']==hip]['col3'])
eteff = np.float(params[params['col1']==hip]['col4'])
unteff = teff + eteff
logg = np.float(params[params['col1']==hip]['col5'])  #gravity
micro = np.float(params[params['col1']==hip]['col7']) #micro turbulence
feh = np.float(params[params['col1']==hip]['col9']) - 7.55 #metallicity

stars = Table.read('714stars_synt.tfits',format='fits')
velshift = np.float(stars[stars['HIP']==hip]['velshift'])  accordingly
finalrot = np.float(stars[stars['HIP']==hip]['finalrot'])
runnr = np.float(stars[stars['HIP']==hip]['runnr'])

carbonlines = [5052.164,5380.335,6587.606,7111.467,7113.177]

if (runnr >= 17) & (runnr<=19):
    t = fits.open('spectra\HIP'+str(hip)+'_red_merged.fits')
    resolv = 55000
if (runnr >= 1) & (runnr<=4):
    t = fits.open('spectra\HIP'+str(hip)+'_red_merged.fits')
    resolv = 65000
if (runnr == 5):
    t = fits.open('spectra\HIP'+str(hip)+'_red_merged.fits')
    resolv = 42000

crpix1 = t[0].header['CRPIX1']
cdelt1 = t[0].header['CDELT1']
```

```
crval1 = t[0].header['CRVAL1']
       #             flux1       f2      f3     f4    f5
fluxer =  np.array([[5051.2, 5379.8, 6587.1, 7110.3, 7112.4],
                    [5051.3, 5380.1, 6587.3, 7110.6, 7112.7],
                    [5054.1, 5381.3, 6588.5, 7111.8, 7113.8],
                    [5054.2, 5381.5, 6588.7, 7111.9, 7114.2]])
inters = fluxer[:, ls]
w_l1, w_l2, w_r1, w_r2 = inters
flux = t[0].data
t.close()
wave = (np.arange(len(flux)) - crpix1+1) * cdelt1 + crval1
wave = wave + wave*(velshift/299792.458)
select = ((wave > w_l1) & (wave < w_l2)) | ((wave > w_r1) & (wave < w_r2))
cont = np.median(flux[select]) #cont 1,2,3,4,5
if ls == 0:
    cont = 1.0
flux = flux/cont   #flux 1,2,3,4,5 for all 5 wavelengths

sme = SME.SME_Structure()
nmu = 7
sme.mu = np.flipud(np.sqrt(0.5*(2*np.arange(nmu)+1)/nmu))
sme.abund = Abund.solar()
sme.atmo.source = "marcs2012p_t2.0.sav"
sme.atmo.method = "grid"
sme.nlte.set_nlte('C', 'nlte_C_scatt_pysme.g.rd')
#sme.nlte.remove_nlte('C')

lines = carbonlines

sme.wran = [int(lines[ls]-3), int(lines[ls]+3)]
sme.linelist = ValdFile("C{}.lin".format(int(lines[ls])))  #vald.linelist
sme.ipres, sme.iptype = resolv, "gauss"
sme.teff, sme.logg, sme.monh, sme.vmic = teff, logg, feh, micro
sme.vsini = 0.1
sme.vmac= finalrot

xvals = np.arange(lines[ls]-10, lines[ls]+10, 0.05)
yvals2 = np.interp(xvals,wave,flux) # observed spectrum
yvals = np.zeros((10,len(xvals)))

for i in np.arange(10):
    sme.abund.update_pattern({"C" : 7.2+0.2*i-sme.monh})
    sme = synthesize_spectrum(sme)
```

```
        swave = sme.wave[0] #synthetic
        sflux = sme.synth[0]
        yvals[i] = np.interp(xvals,swave,sflux)

    ydiff = yvals - yvals2
    ydiffabs = np.abs(ydiff)

    abundances = np.arange(7, 9, 0.2) #try narrower steps
    chi2s = np.zeros(10) # 10 synthetic spectras
    sel = (lines[ls]-0.3 < xvals) & (xvals < lines[ls]+0.3)
    for i in np.arange(10):
        chi2s[i] = np.sum(ydiffabs[i][sel])
    min_chi = np.min(chi2s)
    min_abund = abundances[np.where(chi2s == min_chi)[0][0]]
specrtrum
    i_min = int(np.round((min_abund-7) / 0.2))
    abundances2 = np.arange(np.min(abundances), np.max(abundances),0.01)
    f2 = interp1d(abundances, chi2s, kind='cubic')
    chi2s_f2 = f2(abundances2)

    abundy = np.where(chi2s_f2 == np.min(chi2s_f2))
    min_abund2 = abundances2[abundy][0]
    fig = plt.figure(figsize=(8,9))
    plt.clf()
    save_results_to = '/Users/calum/Desktop/Thesis/TB_Analysis/Pictures/ HIP={}, ls={}'.
    # PLOTS
    def plotter(xvals, yvals, axis, shift, ymin, ymax, vline=True, fluxT=True):
        ax = fig.add_axes(axis)
        ax.cla()
        plt.axis([lines[ls]-shift,lines[ls]+shift,ymin,ymax])
        if fluxT:
            plt.plot(wave,flux,'r')
        if vline and ls != 0 :
            plt.vlines(lines[ls],1,1.1,'k')
            plt.vlines(lines[ls] + 0.3,0.4,1.1,'r', lw = 0.4,linestyles = ':')
            plt.vlines(lines[ls] - 0.3,0.4,1.1,'r', lw = 0.4,linestyles = ':')
        plt.plot(xvals,yvals[i_min],'b')
        for i in inters:
            plt.vlines(i,0.4,1.1,'k', lw=0.3, linestyles = ':')
        for i in np.arange(10):
            plt.plot(xvals,yvals[i],'k',lw=0.5)
    plotter(xvals, yvals, axis=[0.1, 0.6, 0.85, 0.2], shift=4, ymin=0.4, ymax=1.1)
    plt.text(lines[ls],2.0,'HIP '+str(hip)+'',ha='center',fontsize=18)
```

```
plt.text(lines[ls]-3.5,1.7,'Teff = {:.0f} K'.format(teff),fontsize=14)
plt.text(lines[ls]-3.5,1.5,'log g = {:.2f}'.format(logg),fontsize=14)
plt.text(lines[ls]-3.5,1.3,'[Fe/H] = {:.2f}'.format(feh),fontsize=14)
plotter(xvals, yvals, axis=[0.1, 0.35, 0.4, 0.2], shift=1, ymin=0.5, ymax=1.1)
plotter(xvals, ydiff, axis=[0.1, 0.1, 0.4, 0.2], shift=1, ymin=-0.4, ymax=0.4,
    vline=False, fluxT=False)
ax = fig.add_axes([0.57, 0.15, 0.35, 0.3])
plt.axis([6.9,8.9,0,1])
plt.plot(abundances,chi2s,'r.')
plt.plot(abundances2, chi2s_f2)
plt.plot
plt.text(7,0.9, r'Best Abund = {:.2f}'.format(min_abund2), fontsize=14)
plt.axvline(min_abund2) #best abundance
plt.savefig(save_results_to, dpi=100)

return round(min_abund2, 4)
```